Controlled Optimization of Mode Conversion from Electron Bernstein Waves to Extraordinary Mode in Magnetized Plasma

B. Jones,[1] P. C. Efthimion,[1] G. Taylor,[1] T. Munsat,[1] J. R. Wilson,[1] J. C. Hosea,[1] R. Kaita,[1] R. Majeski,[1] R. Maingi,[2] S. Shiraiwa,[3] J. Spaleta,[1] and A. K. Ram[4]

[1]*Princeton Plasma Physics Laboratory, Princeton University, Princeton, New Jersey 08543*
[2]*Oak Ridge National Laboratory, Oak Ridge, Tennessee 37831*
[3]*Graduate School of Frontier Sciences, University of Tokyo, Tokyo 113-0033, Japan*
[4]*Plasma Science and Fusion Center, Massachusetts Institute of Technology, Cambridge, Massachusetts 02139*

(Received 23 January 2002; published 25 April 2003)

In the CDX-U spherical torus, agreement between radiation temperature and Thomson scattering electron temperature profiles indicates ~100% conversion of thermally emitted electron Bernstein waves to the *X* mode. This has been achieved by controlling the electron density scale length (L_n) in the conversion region with a local limiter outside the last closed flux surface, shortening L_n to the theoretically required value for optimal conversion. From symmetry of the conversion process, prospects for efficient coupling in heating and current drive scenarios are strongly supported.

DOI: 10.1103/PhysRevLett.90.165001 PACS numbers: 52.55.Fa, 52.35.Hr, 52.35.Mw, 52.70.Gw

Mode conversion between the electrostatic electron Bernstein wave (EBW) and electromagnetic *X*- and *O*-mode waves is a topic of recent interest, both for its potential applications in controlled fusion research and its relevance to astrophysical phenomena. The EBW propagates across magnetic field lines in a hot plasma and is comprised of longitudinal electric field and electron density oscillations. The EBW is a kinetic mode in which finite electron temperature allows wave propagation, and wave absorption and thermal generation at local electron cyclotron resonances. Additionally, a mode conversion layer surrounds a plasma where the EBW can transform into an *X*- or *O*-mode polarized electromagnetic wave. Coupling of this sort has been invoked to explain emission from astrophysical plasmas [1–5] and absorption in laser produced plasmas [6,7].

In magnetic fusion, the interest in EBW mode conversion is twofold. First, a thermally excited EBW can be measured via mode conversion in order to measure the electron temperature (T_e) of an overdense plasma ($f_{pe} \gg f_{ce}$) for which standard electron cyclotron emission (ECE) techniques [8] are not applicable. This has been performed on the W7-AS stellarator in the case of EBW to *O*-mode conversion via the slow *X* mode (*B-X-O* process), with results in good agreement with theory [9]. In high-β plasmas [including the spherical torus (ST), reversed-field pinch (RFP), or even magnetized process plasmas], lower f_{ce} harmonic electromagnetic waves are evanescent in the plasma core, and accessible higher harmonics do not meet the blackbody emission condition of optical thickness $\tau > 2$. The EBW can propagate above critical density and is strongly absorbed at f_{ce} harmonics with $\tau \approx 300$ in CDX-U [10–12]. An EBW diagnostic has the same potential advantage over Thomson scattering T_e measurement as ECE: it offers a higher data rate with simpler instrumentation. Secondly, the inverse process may be used to heat the plasma or drive current by launching an electromagnetic wave that mode converts and damps as an EBW [13–15]. Electron heating due to mode conversion of a launched *X*-mode wave has recently been observed in the WT-3 tokamak [16], and *O*-mode heating has been studied on W7-AS [17]. In current drive schemes, localized damping of the EBW offers the possibility of tailoring the current profile to stabilize edge modes in an RFP [14]. Noninductive current drive is also of interest in an ST, where operating without the Ohmic solenoid would allow access to lower aspect ratios.

This Letter reports results from an experimental study of EBW to *X*-mode conversion (*B-X*) directed at developing a T_e diagnostic and assessing the prospects for EBW heating and current drive. This work is performed in the CDX-U ST ($R_0 = 34$ cm, $R_0/a \sim 1.5$, $B_{T0} = 0.21$ T, $n_{e0} \sim 4 \times 10^{13}$ cm^{-3}, and $f_{pe}/f_{ce} = 3$–10). It is important to note that the same physics governs *B-X* and *X-B* conversion [18]. Thus, a demonstration of efficient *B-X* conversion validates the prospect of *X-B* heating/current drive. Although *B-X* conversion is also being studied on the Madison Symmetric Torus RFP [19], the unique aspect of the work reported here is that it investigates the *B-X* theory of [20] in detail while controlling and optimizing the *B-X* conversion through the implementation of a local limiter. This is possible because the mode conversion for lower f_{ce} harmonic EBWs typically occurs outside the last closed flux surface (LCFS) in an ST. Consequently, the electron density profile in this region can be modified by material limiters.

B-X conversion occurs for $n_\parallel \approx 0$ with a mode conversion efficiency (C) sensitively dependent on L_n in the conversion region at the upper-hybrid resonance (UHR). A 1D slab model results in the analytic theory for $n_\parallel = 0$ presented in [20]. The full expression for mode conversion

 © 2003 The American Physical Society

efficiency is

$$C = C_{\max} \cos^2(\phi/2 + \theta), \quad (1)$$

where $\cos^2(\phi/2 + \theta)$ is a factor relating to the phasing of the waves in the mode conversion region with $\theta = \arg\Gamma(-i\eta/2)$, and ϕ evaluated in the manner of [21] for the case of the high-field cutoff close to resonance. The maximum mode conversion efficiency ($C_{\max}$) is given by

$$C_{\max} = 4e^{-\pi\eta}(1 - e^{-\pi\eta}). \quad (2)$$

When the magnetic scale length in the mode conversion region $L_B \gg L_n$ as in CDX-U,

$$\eta \approx [2\pi f_{ce} L_n/(c\alpha)][(1 + \alpha^2)^{1/2} - 1]^{1/2}, \quad (3)$$

where f_{ce}, L_n, and $\alpha = f_{pe}/f_{ce}$ are evaluated at the UHR layer. Obtaining $C \sim 100\%$, or equivalently radiation temperature $T_{\text{rad}} \sim T_e$, requires $L_n \approx 0.5$ cm in CDX-U. Optimizing C is also desirable for EBW heating/current drive. This conversion is expected to be less sensitively dependent on $n_\parallel$ than *O-X-B* conversion, as that process requires finite $n_\parallel$ that is a function of the plasma parameters [22].

Two absolutely calibrated, heterodyne radiometers measured fundamental (4–8 GHz) and second harmonic (8–12 GHz) EBW emission every 20 μs in CDX-U [23]. Localization of the EBW emission source to the f_{ce} resonant surfaces was verified by observing the response of the T_{rad} profile to cooling gas puffs [9,24]. This justifies a comparison between the measured T_{rad} and Thomson scattering T_e profiles in order to infer a value of C. In previous experiments with an antenna outside a vacuum window, $C \sim 10\%$ was observed [15]. Similar observations have been made on the National Spherical Torus Experiment [25].

Rather than relying on the density profile naturally provided by the plasma, it is necessary to create a shorter L_n at the UHR layer outside the LCFS in order to reach $C \sim 100\%$. To meet this goal, an in-vacuum quad-ridged horn antenna [26] along with a movable local limiter was installed in CDX-U, shown in Fig. 1. The antenna points perpendicular to the LCFS ($n_\parallel = 0$) on the outboard midplane. Huygen's principle modeling with a Green's function formalism [27] assuming a TE_{10} mode implies antenna sensitivity to waves with $n_\parallel \ll 0.1$. Full-wave numerical calculation [20] indicates variation in C of order $\sim 1\%$ for $0 < n_\parallel < 0.1$, so $n_\parallel = 0$ *B-X* theory is applicable. An *X* mode T_{rad} 3 times greater than the *O* mode T_{rad} is measured, consistent with *B-X* theory including calculated *B-X-O* coupling to the *O*-mode antenna. The local limiter shortens L_n in the scrape-off layer (SOL) where the *B-X* mode conversion occurs for f_{ce} and 2 f_{ce} and is not the primary limiter for the plasma. Also shown in Fig. 1, an array of Langmuir probes measures L_n in the mode conversion region so that C can be calculated from Eq. (1). These probes can be swept to measure T_e or biased negatively to measure electron density (n_e).

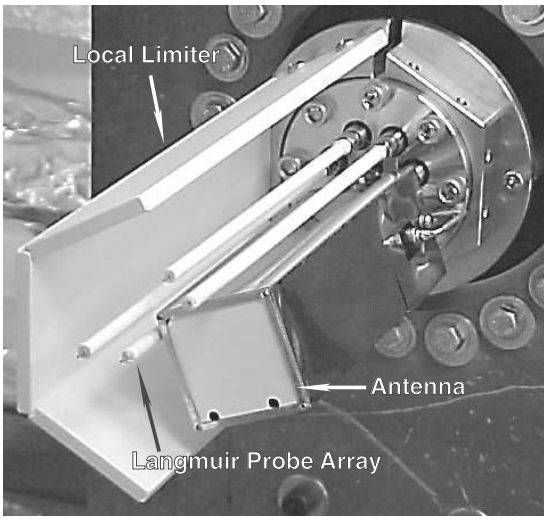

FIG. 1. The CDX-U EBW diagnostic combines a quad-ridged horn antenna to measure emission, a movable local limiter (half shown) to modify L_n in front of the antenna to optimize mode conversion, and a Langmuir probe array to measure L_n.

Figure 2(a) shows the significant shortening of L_n outside the LCFS due to the local limiter, with data averaged over 0.1 ms to smooth out fluctuations. With the local limiter located near the LCFS, an average density scale length $L_n = 0.66 \pm 0.07$ cm was measured (triangles, solid line). The profile naturally occurring in the SOL was measured to have $L_n = 3$–6 cm (diamonds, dashed line).

Using these density profiles, the UHR frequency $f_{\text{UH}} = (f_{pe}^2 + f_{ce}^2)^{1/2}$ is calculated as a function of major radius in Fig. 2(b). An EBW of a given frequency mode converts when the outgoing wave reaches the radial position at which $f = f_{\text{UH}}$. With the local limiter present (solid line), the mode conversion for 4–12 GHz occurs in the few-centimeter-wide region between the limiter and antenna. The corresponding right- (f_R) and left-hand (f_L) cutoffs are shown (dotted lines), which bound the mode conversion region. The *X* mode is evanescent between f_{UH} and f_R, and this tunneling distance shortens from several centimeters to a few millimeters in the presence of the local limiter.

The effect of the local limiter on the EBW emission is seen in Fig. 3. With the antenna at $R = 68$ cm so that the mode conversion occurs in a region with long L_n, the fundamental emission is observed at a low level (triangles). With the local limiter near the LCFS so that the mode conversion occurs in a region of short L_n, the emission increased by an order of magnitude (diamonds, solid line). We also plot the second harmonic T_{rad} (diamonds, dashed line), and note that there is favorable

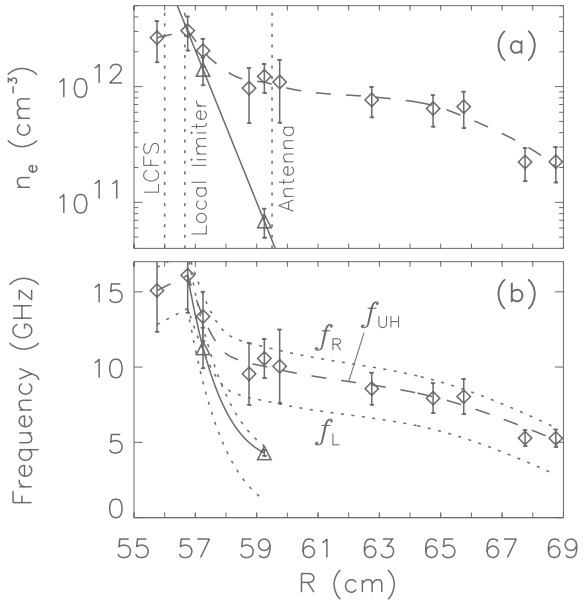

FIG. 2. (a) The $L_n = 3$–6 cm electron density profile naturally occurring in the SOL (diamonds, dashed line) and the $L_n = 0.66 \pm 0.07$ cm profile created by the local limiter (triangles, solid line). (b) The corresponding UHR frequency profiles, and left- and right-hand cutoffs (dotted lines) that define the mode conversion region.

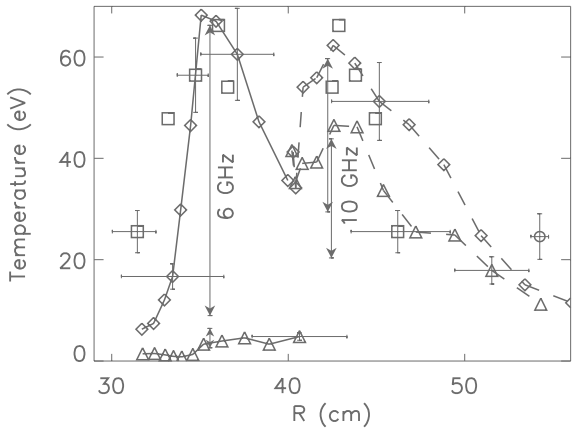

FIG. 3. The radiation temperature without the local limiter (triangles). With the local limiter, the peak fundamental emission (diamonds, solid line) and second harmonic emission (diamonds, dashed line) together map out the T_e profile and are consistent with T_e measured by Thomson scattering (squares) and Langmuir probe (circle). Error bars are shown for selected points. The emission fluctuation levels at 6 and 10 GHz are indicated by vertical arrowed lines.

agreement with Thomson scattering (squares) and Langmuir probe (circle) T_e data for both fundamental and second harmonic mode-converted EBW emission with L_n shortened by the local limiter. The hollow temperature profile is typical and is expected as CDX-U plasma duration is only ~15 ms. A less dramatic reduction in second harmonic $T_{\rm rad}$ is seen without the local limiter, due to the natural steepening of L_n near the LCFS seen in Fig. 2.

The nominal f_{ce} harmonic location is the position of the inboard R error bar. The outboard error bar position is that of the Doppler-shifted cyclotron harmonic of a ray launched 3 cm off midplane, calculated with the GENRAY ray tracing code [28]. This 3 cm shift reflects the uncertainty in the vertical position of the plasma, measured with the CDX-U poloidal soft x-ray array [29]. Radiometer bandwidth dominated this effect for $R >$ 50 cm. Note that GENRAY indicates insensitivity of the emission location to $n_\parallel$ at the antenna for $0 < n_\parallel < 0.1$. 15% $T_{\rm rad}$ error bars are due to systematic error in the absolute calibration, performed using Dicke switching of a blackbody source. The Thomson scattering measurements are taken along a vertical axis (z) at a fixed beam radial position and mapped from z to R using canonical CDX-U flux surface shapes.

The n_e profile data from the probes and the EBW emission measurements can test the theory of B-X mode conversion presented in [20]. Figure 4 shows the theoretical mode conversion efficiency C calculated from Eq. (1) as a function of L_n at both 6 and 10 GHz (fundamental and second harmonic emission frequencies). The average L_n measured behind the local limiter is shown (dashed vertical line), with the shaded region representing the error bars. It is seen that $C \sim 100\%$ is theoretically attainable with the short L_n produced by the local limiter.

Large fluctuations in the emission signal are observed (Fig. 5(d)). The $T_{\rm rad}$ profiles shown in Fig. 3 represent single radiometer sweeps selected at the peak of fluctuating emission within the analysis time window. Vertical arrowed lines show the peak-to-peak fluctuation at 6 and 10 GHz. Evidence that fluctuating L_n is playing a role in modifying C, leading to fluctuating emission, is seen by

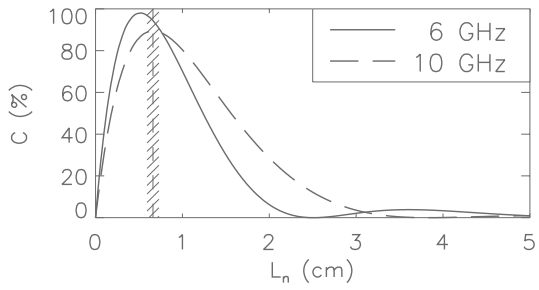

FIG. 4. The theoretical mode conversion efficiency C for 6 GHz (solid line) and 10 GHz (dashed line) emission as a function of L_n just outside the CDX-U LCFS. The measured L_n (vertical line) is consistent with optimized B-X conversion.

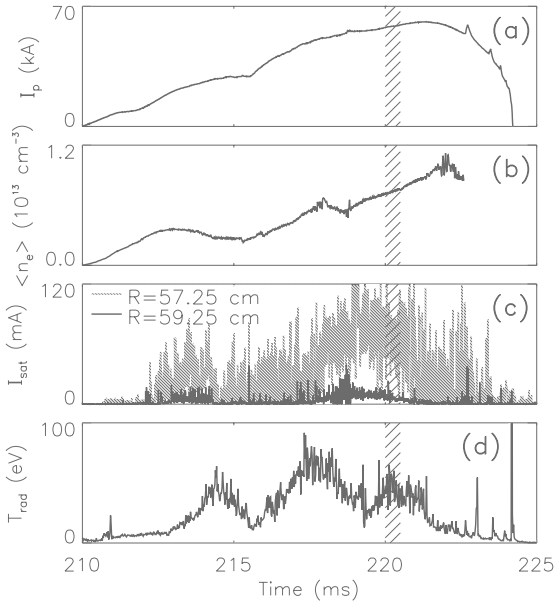

FIG. 5. Time evolution of a typical CDX-U discharge. (a) Toroidal plasma current, (b) line-averaged density ($R =$ 35 cm), (c) ion saturation current from Langmuir probes showing edge n_e fluctuation (local limiter at $R = 56.6$ cm, data from two separate shots), and (d) EBW T_{rad} at 10 GHz, showing multiple peaks resulting from gas puff modulation and fluctuation resulting from changing L_n. Analysis was performed in the shaded time window.

comparing the T_{rad} and probe I_{sat} time evolution. For several probe tip positions, the cross correlation between these signals was calculated in a time window $\sim$1 ms wide. 70% anticorrelation was observed for the probe located 0.6 cm behind the local limiter and emission at 5.5 GHz, which mode converts near the probe location. The emission peaked when the density behind the limiter dropped, consistent with L_n shortening. Correlation was not seen for probes 2 cm on either side of this location, suggesting that the T_{rad} fluctuation was caused by density fluctuation local to the UHR layer.

Variation in L_n is not the only factor leading to T_{rad} fluctuation. One additional effect is changing refraction of the emitted EBW. GENRAY calculations indicate that the EBW emission location viewed is sensitive to the vertical position of the plasma. Correlation between fluctuations in T_{rad} and strong MHD activity may indicate the emission location is oscillating across a region of varying T_e as the changing plasma profile modulates the EBW ray paths.

100% *B-X* mode conversion efficiency has been observed in CDX-U by controlling L_n at the UHR layer, allowing direct measurement of the T_e profile from mode-converted EBW emission. The measured T_e profile was similar to that measured by Thomson scattering. $C \sim$ 100% and measured L_n at the UHR are consistent with the theory of [20]. Since the mode conversion occurs in the SOL for an ST, L_n can be controlled and optimized with a local limiter that does not perturb the plasma. Similarly, symmetry of the mode conversion process is a strong justification for using a local limiter with an *X*-mode electromagnetic heating or current drive antenna to achieve efficient coupling to the EBW branch.

The authors would like to thank the CDX-U technical staff and T. Kramer for their contributions. This work was supported by DOE Contracts No. DE-AC02-76-CHO-3073 as part of the "Innovations in Magnetic Fusion Energy Diagnostic Systems" program, No. DE-FG02-91ER-54109, and No. DE-FG02-99ER-54521.

[1] T. B. Leyser *et al.*, Phys. Rev. Lett. **63**, 1145 (1989).
[2] P. Stubbe and H. Kopka, Phys. Rev. Lett. **65**, 183 (1990).
[3] P. A. Bernhardt *et al.*, Phys. Rev. Lett. **72**, 2879 (1994).
[4] S. P. Kuo, Phys. Plasmas **4**, 3194 (1997).
[5] T. Haruki and J.-I. Sakai, Astrophys. J. **552**, L175 (2001).
[6] C. Grebogi *et al.*, Phys. Rev. Lett. **39**, 338 (1977).
[7] W. Woo, K. Estabrook, and J. S. DeGroot, Phys. Rev. Lett. **40**, 1094 (1978).
[8] M. Bornatici *et al.*, Nucl. Fusion **23**, 1153 (1983).
[9] H. P. Laqua *et al.*, Phys. Rev. Lett. **81**, 2060 (1998).
[10] P. C. Efthimion *et al.*, Rev. Sci. Instrum. **70**, 1018 (1999).
[11] J. Hosea, V. Arunasalam, and R. Cano, Phys. Rev. Lett. **39**, 408 (1977).
[12] T. Jones, Ph.D. thesis, Princeton University, 1995.
[13] N. J. Fisch and A. H. Boozer, Phys. Rev. Lett. **45**, 720 (1980).
[14] C. B. Forest *et al.*, Phys. Plasmas **7**, 1352 (2000).
[15] G. Taylor *et al.*, AIP Conf. Proc. **595**, 282 (2001).
[16] T. Maekawa *et al.*, Phys. Rev. Lett. **86**, 3783 (2001).
[17] H. P. Laqua *et al.*, Phys. Rev. Lett. **78**, 3467 (1997).
[18] A. K. Ram, A. Bers, and C. N. Lashmore-Davies, Phys. Plasmas **9**, 409 (2002).
[19] P. K. Chattopadhyay *et al.*, AIP Conf. Proc. **595**, 346 (2001).
[20] A. K. Ram and S. D. Schultz, Phys. Plasmas **7**, 4084 (2000).
[21] A. K. Ram, A. Bers, and S. D. Schultz, Phys. Plasmas **3**, 1976 (1996).
[22] J. Preinhaelter and V. Kopecky, J. Plasma Phys. **10**, 1 (1973).
[23] G. Taylor *et al.*, Rev. Sci. Instrum. **72**, 285 (2001).
[24] T. Munsat *et al.*, Phys. Plasmas **9**, 480 (2002).
[25] G. Taylor *et al.*, Phys. Plasmas **9**, 167 (2002).
[26] K. L. Walton and V. C. Sundberg, Microw. J. **7**, 96 (1964).
[27] J. A. Kong, *Electromagnetic Wave Theory* (John Wiley & Sons, New York, 1986).
[28] R. W. Harvey, M. G. McCoy, and G. D. Kerbel, Phys. Rev. Lett. **62**, 426 (1989).
[29] D. Stutman *et al.*, Rev. Sci. Instrum. **68**, 1059 (1997).